Research Article | Vol. 7, No. 8 | 1 Aug 2017 | OPTICAL MATERIALS EXPRESS 3041
Optical Materials EXPRESS

Strong near band edge emission of (Ce, Yb) co-doped ZnO thin films after high temperature annealing

C. L. HENG,[1,4] W. XIANG,[1] W. Y. SU,[1] H. C. WU,[1] Y. K. GAO,[2] P. G. YIN,[2] AND T. G. FINSTAD[3,5]

[1]*School of Physics, Beijing Institute of Technology, Beijing 100081, and State Key Laboratory for Artificial Microstructure & Mesoscopic Physics, Peking University, Beijing 100871, China*
[2]*Key Laboratory of Bio-Inspired Smart Interfacial Science and Technology of Ministry of Education, School of Chemistry and Environment, Beihang University, Beijing 100191, China*
[3]*Physics Department, University of Oslo, PO Box 1048, Blindern, N-0316, Oslo Norway*
[4]*hengcl@bit.edu.cn*
[5]*terje.finstad@fys.uio.no*

Abstract: We studied the photoluminescence (PL) properties of (Ce + Yb) co-doped ZnO thin films as a function of high temperature annealing. The films were fabricated by magnetron sputtering. After 1000-1100°C annealing, the near band edge (NBE) emissions of the films were dozens to a hundred times stronger than that of undoped ZnO, while the Yb^{3+} emission (~980 nm) was quite weak, indicating that energy transfers from the ZnO host to Yb^{3+} ions in the films were not efficient. X-ray diffraction analysis and scanning electron microscopy observations demonstrated that the (Ce + Yb) co-doping had a large effect on the morphology and crystallinity of the films. The crystallinity enhancement of the films is considered to be the main reason for the strong NBE enhancements of the co-doped ZnO films.

OCIS codes: (310.3840) Materials and process characterization; (260.7190) Ultraviolet; (160.5690) Rare-earth-doped materials; (260.3800) Luminescence.

References and links

1. S. Ye, F. Xiao, Y. X. Pan, Y. Y. Ma, and Q. Y. Zhang, "Phosphors in phosphor-converted white light-emitting diodes: recent advances in materials, techniques and properties," Mater. Sci. Eng. Rep. **71**(1), 1–34 (2010).
2. H. Dong, L.-D. Sun, and C.-H. Yan, "Energy transfer in lanthanide upconversion studies for extended optical applications," Chem. Soc. Rev. **44**(6), 1608–1634 (2015).
3. X. F. Wang, Q. Liu, Y. Y. Bu, C.-S. Liu, T. Liu, and X. H. Yan, "Optical temperature sensing of rare-earth ion doped phosphors," RSC Advances **5**(105), 86219–86236 (2015).
4. Y. Zhang, Y. Liu, X. Li, Q. J. Wang, and E. Xie, "Room temperature enhanced red emission from novel Eu^{3+} doped ZnO nanocrystals uniformly dispersed in nanofibers," Nanotechnology **22**(41), 415702 (2011).
5. V. Kumar, S. Som, V. Kumar, V. Kumar, O. M. Ntwaeaborwa, E. Coetsee, and H. C. Swart, "Tunable and white emission from ZnO:Tb^{3+} nanophosphors for solid state lighting applications," Chem. Eng. J. **255**(7), 541–552 (2014).
6. M. Balestrieri, G. Ferblantier, S. Colis, G. Schmerber, C. Ulhaq-Bouillet, D. Muller, A. Slaoui, and A. Dinia, "Structural and optical properties of Yb-doped ZnO films deposited by magnetron reactive sputtering for photon conversion," Sol. Energy Mater. Sol. Cells **117**(4), 363–371 (2013).
7. W. Q. Zou, C. N. Ge, G. Venkataiah, H. L. Su, H. S. Hsu, J. C. A. Huang, X. C. Liu, F. M. Zhang, and Y. W. Du, "Ferromagnetism in Tb doped ZnO nanocrystalline films," J. Appl. Phys. **111**(11), 113704 (2012).
8. A. J. Steckl, J. C. Heikenfeld, D. S. Lee, M. J. Garter, C. C. Baker, Y. Q. Wang, and R. Jones, "Rare-earth-doped GaN: growth, properties, and fabrication of electroluminescence devices," IEEE J. Sel. Top. Quantum Electron. **8**(4), 749–766 (2002).
9. S. M. Ahmed, P. Szymanski, L. M. El-Nadi, and M. A. El-Sayed, "Energy-transfer efficiency in Eu-doped ZnO thin films: the effects of oxidative annealing on the dynamics and the intermediate defect states," ACS Appl. Mater. Interfaces **6**(3), 1765–1772 (2014).
10. S. Geburt, M. Lorke, A. L. da Rosa, T. Frauenheim, R. Röder, T. Voss, U. Kaiser, W. Heimbrodt, and C. Ronning, "Intense intrashell luminescence of Eu-doped single ZnO nanowires at room temperature by implantation created Eu-O_i complexes," Nano Lett. **14**(8), 4523–4528 (2014).

#295136 https://doi.org/10.1364/OME.7.003041
Journal © 2017 Received 2 May 2017; revised 18 Jul 2017; accepted 22 Jul 2017; published 31 Jul 2017

Optical Materials EXPRESS

11. M. V. Shestakov, A. N. Baranov, V. K. Tikhomirov, Y. V. Zubavichus, A. S. Kuznetsov, A. A. Veligzhanin, A. Y. Kharin, R. Rösslhuber, V. Y. Timoshenko, and V. V. Moshchalkov, "Energy-transfer luminescence of a zinc oxide/ytterbium oxide nanocomposite," RSC Advances **2**(23), 8783–8788 (2012).
12. L. Yang, J. Z. Dong, Z. C. Jiang, A. L. Pan, and X. J. Zhuang, "Visible light stimulating dual-wavelength emission and O vacancy involved energy transfer behavior in luminescence for coaxial nanocable arrays," J. Appl. Phys. **115**(22), 224308 (2014).
13. L. V. Gritsenko, Kh. A. Abdullin, M. T. Gabdullin, Zh. K. Kalkozova, S. E. Kumekov, Zh. O. Mukash, A. Yu. Sazonov, and E. I. Terukov, "Effect of thermal annealing on properties of polycrystalline ZnO thin films," J. Cryst. Growth **457**, 164–170 (2017).
14. H. Kind, H. Q. Yan, B. Messer, M. Law, and P. D. Yang, "Nanowire ultraviolet photodetectors and optical switches," Adv. Mater. **14**(2), 158–160 (2002).
15. H. S. Kim, F. Lugo, S. J. Pearton, D. P. Norton, Y. L. Wang, and F. Ren, "Phosphorus doped ZnO light emitting diodes fabricated via pulsed laser deposition," Appl. Phys. Lett. **92**(11), 112108 (2008).
16. Y. R. Ryu, J. A. Lubguban, T. S. Lee, H. W. White, T. S. Jeong, C. J. Youn, and B. J. Kim, "Excitonic ultraviolet lasing in ZnO-based light emitting devices," Appl. Phys. Lett. **90**(13), 131115 (2007).
17. Q. Yu, T. T. Ai, L. Y. Jiang, Y. T. Zhang, C. Li, and X. Q. Yuan, "Efficient energy transfer in Eu-doped ZnO on diamond film," RSC Advances **4**(96), 53946–53949 (2014).
18. L. Luo, L. Gong, Y. F. Liu, J. Chen, C. R. Ding, X. G. Tang, X. L. Li, Z. R. Qiu, H. Z. Wang, X. M. Chen, K. F. Li, H. H. Fan, and K. W. Cheah, "Enhanced ultraviolet lasing from europium-doped zinc oxide nanocrystals," Opt. Mater. **32**(9), 1066–1070 (2010).
19. C. L. Heng, T. Wang, H. Li, J. J. Liu, A. Ablimit, W. Y. Su, H. C. Wu, P. G. Yin, and T. G. Finstad, "Strong enhancement of ultra-violet emission by Ce doping of ZnO sputtered films," Mater. Lett. **162**, 53–55 (2016).
20. C. L. Heng, T. Wang, W. Y. Su, H. C. Wu, M. C. Yang, L. G. Deng, P. G. Yin, and T. G. Finstad, "Intense ultraviolet photoluminescent emission from Yb doped ZnO thin films on Si after high temperature annealing," J. Alloys Compd. **695**, 2232–2237 (2017).
21. U. Özgür, Y. I. Alivov, C. Liu, A. Teke, M. A. Reshchikov, S. Doğan, V. Avrutin, S. J. Cho, and H. Morkoc, "A comprehensive review of ZnO materials and devices," J. Appl. Phys. **98**(4), 041301 (2005).
22. J. K. Larsen, S.-Y. Li, J. J. S. Scragg, Y. Ren, C. Hägglund, M. D. Heinemann, S. Kretzschmar, T. Unold, and C. Platzer-Björkman, "Interference effects in photoluminescence spectra of Cu_2ZnSnS_4 and $Cu(In,Ga)Se_2$ thin films," J. Appl. Phys. **118**(3), 035307 (2015).
23. M. García-Méndez, R. R. Segura, V. Coello, E. M. Guerra, and A. Bedoya-Calle, "The influence of Ce doping on the structural and optoelectronic properties of RF-sputtered ZnO films," Opt. Quantum Electron. **47**(8), 2637–2648 (2015).
24. W. E. Mahmoud, "Synthesis and optical properties of Ce-doped ZnO hexagonal nanoplatelets," J. Cryst. Growth **312**(21), 3075–3079 (2010).
25. Y. Morinaga, K. Sakuragi, N. Fujimura, and T. Ito, "Effect of Ce doping on the growth of ZnO thin films," J. Cryst. Growth **174**(1), 691–695 (1997).
26. N. Jiang, S. Ye, and J. R. Qiu, "Electron energy-loss spectroscopy study of Yb doped ZnO," J. Appl. Phys. **108**(8), 083535 (2010).
27. S. Ye, N. Jiang, F. He, X. Liu, B. Zhu, Y. Teng, and J. R. Qiu, "Intense near-infrared emission from ZnO-$LiYbO_2$ hybrid phosphors through efficient energy transfer from ZnO to Yb^{3+}," Opt. Express **18**(2), 639–644 (2010).
28. M. V. Shestakov, V. K. Tikhomirov, D. Kirilenko, A. S. Kuznetsov, L. F. Chibotaru, A. N. Baranov, G. Van Tendeloo, and V. V. Moshchalkov, "Quantum cutting in Li (770 nm) and Yb (1000 nm) co-dopant emission bands by energy transfer from the ZnO nano-crystalline host," Opt. Express **19**(17), 15955–15964 (2011).
29. J. Lin, Y. Fujita, and A. Neogi, "Saturation of two photon emission in ZnO nanoparticles with second order nonlinearity," RSC Advances **5**(15), 10921–10926 (2015).
30. G. P. He, H. Q. Fan, and Z. W. Wang, "Enhanced optical properties of heterostructured ZnO/CeO_2 nanocomposite fabricated by one-pot hydrothermal method: fluorescence and ultraviolet absorption and visible light transparency," Opt. Mater. **38**, 145–153 (2014).

1. Introduction

There are several reviews on the applications of rare earth elements (REs) in various host materials used for optical applications such as upconversion of photons, color conversion or thermometry [1–3]. REs have unfilled 4f shell structures with many energy levels and meta-stable states, which can be used to emit various luminescent wavelengths with narrow luminescent bands. Rare earth (RE) doped ZnO have attracted extensive interest because of the potential applications in photoelectric, magnetic and photo-catalysis devices [4–7]. ZnO has a wide band gap of about 3.37 eV and a large exciton binding energy of 60 meV at room temperature. Inspired by successful incorporation of RE in wide band gap semiconductor GaN for optoelectronic applications [8], many researchers turned to ZnO as a host for RE ions for light emitting devices. But it has not been easy to accommodate RE ions into the ZnO

Optical Materials EXPRESS

lattice due to the mismatch of charge and radius between the RE ion and Zn^{2+}; and even if preferred RE^{3+} ions were somehow introduced into the ZnO lattice, there should still be no efficient light emissions from the RE ions, because the luminescence lifetime of RE ions is at least 10^3 times longer than the excitons decay time in ZnO. In recent years, with the great advances in synthesizing ZnO nano-structures (nano-ZnO), many research groups reported that by modulating the defects (whether extrinsic or intrinsic) of the nano-ZnO to form "energy trap centers", effective energy transfer from the host nano-ZnO to RE ions can be realized [9–12].

On the other hand, acquiring intense ultraviolet (UV) emission from ZnO is always a challenge in ZnO based UV photonics and various methods to enhance the UV emission have been reported [13–16]. REs doping of ZnO and its influence on the near band edge (NBE) emission of ZnO [17, 18] were reported, and a NBE enhancement was observed but the mechanism for the enhancement is not clear. Ce^{3+} can emit blue light and the absorption cross section of the electric-dipole allowed 4f-5d transition is large (of the order of 10^{-18} cm^2), while the radiation from Yb^{3+} (~980 nm) has many important applications. Both are frequently used in dopants-luminescence. Previously, we reported that after high temperature (1000-1100 °C) annealing, the NBE emissions of ZnO films were both enhanced by one to two orders of magnitude after doping with Ce [19] or Yb [20] compared to the undoped case, whereas the structures of the two films were quite different. In the present work, we have investigated further the NBE enhancement effects by co-doping Ce + Yb in the nano-ZnO films with various RE concentrations, and compared the enhancement efficiency with those of single RE doping cases. We have also compared their structural variations after the high temperature annealing, and their effects on the critical excitation power of photoluminescence (PL). The strong NBE emission is our main focus in this report, while the RE emissions are here relatively weak. The strong NBE emissions from the RE doped ZnO may pave a way to develop ZnO UV based photoelectric devices.

2. Experimental

The (Ce + Yb) co-doped ZnO films were deposited by magnetron sputtering using two composite targets. One composite target was ZnO + CeO_2, made by attaching small pieces of CeO_2 on the surface of a ZnO target (purity 99.999%); the other composite target was ZnO + Yb_2O_3, made by placing large ZnO plates on the surface of an Yb_2O_3 target (purity 99.99%). The films were deposited on single crystal Si wafers with a native oxide. The base vacuum pressure was 2.0×10^{-3} Pa. The working gas was a mixture of argon and oxygen with flow rates of 25.0 and 5.0 sccm, respectively. During deposition the gas pressure was kept at 1.3 Pa. No intentional substrate heating was used during the sputtering and the Si substrates were rotated during deposition to obtain lateral uniformity. The sputtering power applied to the ZnO + CeO_2 target was always 120 W, while the power applied to the ZnO + Yb_2O_3 target was kept at 75, 100 or 120 W, to yield different composition of the film called S1, S2 and S3, respectively. For comparison, a reference undoped ZnO film (called S0) was deposited by sputtering only the ZnO target; a control Yb-doped ZnO film (S4) and a Ce-doped ZnO film (S5) [19] with similar Yb (or Ce) doping concentration, were also deposited by sputtering the ZnO + Yb_2O_3 and ZnO + CeO_2 targets, respectively. The power applied to the targets for the control samples were all 120 W. The stoichiometry of the films was characterized by using Rutherford backscattering spectrometry (RBS, NEC 2x1.7 MV Tandem Accelerator in Ion Beam Materials Laboratory in Peking University). The RE doping concentration and the film thickness are shown in Table 1.

The Si wafers with the films were then cleaved into small pieces and annealed at various temperatures in flowing N_2 (purity 99.999%) gas. The crystallinity of the films was examined by X-ray diffraction (XRD) using a D8 ADVANCE diffractometer with Cu $K\alpha_1$ radiation (λ = 1.54056Å). The surface morphology of the films was investigated by scanning electron microscopy (SEM) (German Zeiss Microscope) and the attached energy dispersive X-ray

Optical Materials EXPRESS

spectroscopy (EDS) was used to examine lateral variation of the elements. The PL spectra were recorded by using a Lab RAM HR microscopic fluorescence image system, where the samples were excited using the 325 nm line of a He-Cd laser (~30 mW) and detected by a spectrometer employing a charge-coupled device array. The PL excitation (PLE) spectra were recorded with a FLS 980 fluorescence spectrophotometer. All the measurements were performed at room temperature.

Table 1. The stoichiometry of the sample films

Samples	Zn (at.%)	O (at.%)	Ce (at.%)	Yb (at.%)	Thickness (nm)
S0	46.10	53.90	0	0	890
S1	46.36	53.31	0.09	0.24	575
S2	48.71	50.60	0.14	0.55	485
S3	48.82	49.99	0.31	0.88	495
S4	46.1	53.4	0	0.5	243
S5	47.0	52.9	0.1	0	240

3. Results and discussion

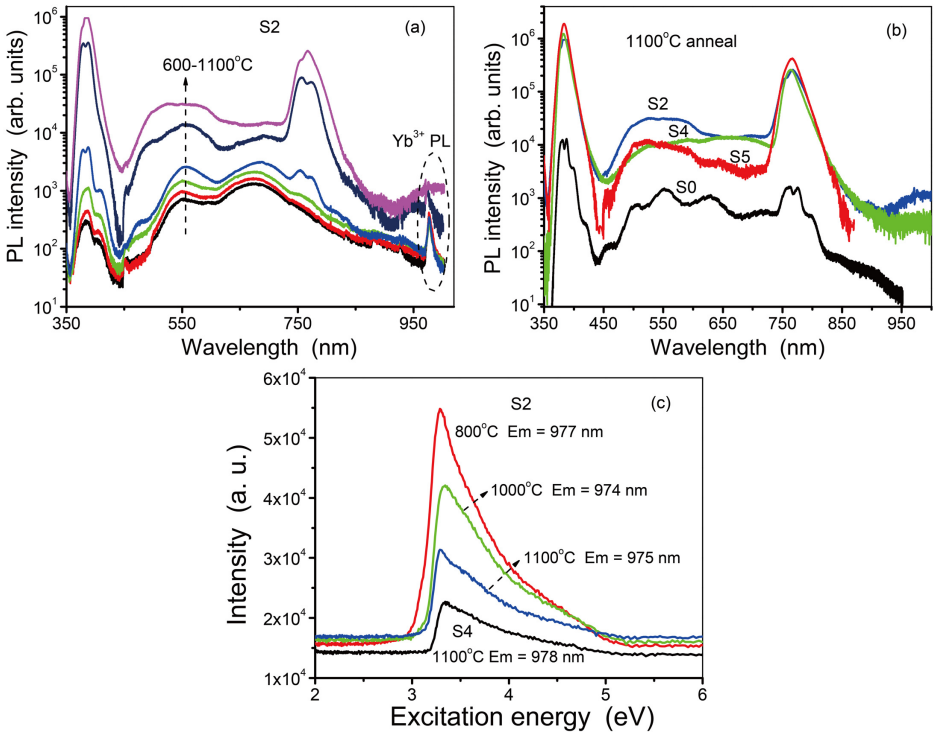

Fig. 1. (a) PL spectra of the S2 film after annealing in N_2 for 30 minutes at the indicated temperatures; (b) PL spectra of S0, S2, S4 and S5 after the identical 1100 °C annealing; (c) PL excitation spectra for the S2 film after 800, 1000 and 1100 °C annealing, respectively, and for the S4 film after the 1100 °C annealing. The monitoring wavelength is at their Yb^{3+} PL emission peak positions.

Optical Materials EXPRESS

Figure 1(a) depicts the PL spectra of sample S2 recorded in the range 350-1000 nm for different anneal temperatures. The 350-450 nm spectral range indicates the near band-edge (NBE) emission of ZnO, while the range 450-700 nm comprises emissions from both the defects and REs ions of the annealed film [19, 20]. The range 700-900 nm includes the second order diffraction (from diffracting grating monochromator) from the NBE emission. Finally the peak at around 977 nm is attributed to the $4f(^2F_{5/2})\rightarrow 4f(^2F_{7/2})$ transition of Yb^{3+}. It should be remarked that some of the spectral variations within each spectrum may be influenced by interference effects from the surface and interface of the film. However, the variation of the intensity among the larger regions themselves as indicated above and which we will consider for annealing effects, will not be influenced much. It is seen that all the PL spectra have NBE emission signal consisting of a peak position at around 385 nm and a shoulder at around 410 nm, and the intensity in this UV region increases much with annealing temperature. The weak Yb^{3+} PL, which does not have as large increase with anneal temperature as the NBE PL, infers that there is no efficient transfer of excitation energy from the host ZnO to Yb^{3+} in the samples. The same may apply for transfer from Ce ions to Yb^{3+}. Samples S1 and S3 have PL curves resembling those of S2. The PL spectrum intensity was very weak after 1200 °C annealing for all the sample types (not shown, but indicating the thermal stability range of the films).

Figure 1(b) compares the PL spectra of sample S0, S2, S4 and S5 films after identical 1100 °C annealing. The S0 film shows a PL spectrum that is typical for undoped ZnO [21]. The wavy fluctuations on the spectrum are considered to be influenced by interference effects [22]. The PL spectra of S2, S4 and S5 have increased significantly in intensity after the REs doping. The spectra of S1 and S3 (not shown) have similar high intensity as S2. More detailed analysis indicates that the S2 film has the strongest visible and Yb^{3+} emission regions among the films, while the control films, S4 and S5, show stronger NBE PL intensity than what the S2 sample does. The difference in the shape of the visible bands for the control samples indicates that the emissions from Ce and Yb ions and/or defects induced by these ions have been involved. Figure 1(c) shows the PLE spectra of S2 and S4 after annealing at the temperatures indicated. The monitoring wavelengths are at the Yb^{3+} emission peak wavelengths. There is an asymmetric excitation band in the range of 3.0-5.0 eV in all the spectra with peak position at around 3.3 eV. The excitation of Yb^{3+} in S2 and S4 could originate from an energy transfer from the ZnO matrix and Ce ions to the Yb^{3+}. Note that the spectra of S2 and S4 are similar to each other. Then, since there is no Ce in S4, it is natural to conclude that energy transfer from Ce ions to Yb^{3+} is not a dominant excitation process for S2. Note that for S2, the intensity of the band decreases with increasing anneal temperature from 800 to 1100 °C.

Figure 2(a) plots the integral intensity of the NBE emission bands (I_{NBE}), in the PL spectra of the samples S0-5 as a function of the annealing temperature. Here I_{NBE} is integrated over the wavelength range of 350-450 nm. I_{NBE} increases with increasing anneal temperature for all the samples, and the increase is much larger for S1-5 than for S0. Notably the NBE intensity increases by four orders of magnitude for sample S3 by going from 600 °C annealing to 1100 °C annealing. And the I_{NBE} for S1-3 are 85, 86, and 89 times, respectively, stronger than that for S0 after the 1100 °C annealing. S4 has comparable NBE intensity as those of S1-S3, while S5 has the strongest NBE intensity among the films. Figure 2(b) shows I_{VIS}, which is the PL intensity integrated between 450 and 700 nm. It is seen that I_{VIS} is stronger for the films S1-5 than for film S0, which could be due to the Ce and/or Yb doping having caused more radiative defects (including the RE itself). Further I_{VIS} also increases with annealing for S1-5 while I_{NBE} has a stronger increase which can be seen clearly from Fig. 2(c) showing the ratio (I_{NBE}/I_{VIS}). All the ratios increase much for annealing at elevated temperature, but samples S1-4 show higher ratios than those of S0, especially for annealing to 1100 °C. Notably S5 has the highest ratios among the films at all the temperatures. Generally, the increase of the I_{NBE}/I_{VIS} ratio is often regarded to be due to the film crystal quality being

Optical Materials EXPRESS

improved [23], while some caution should be exercised in using that approximate general tendency to compare situations. Here, the improvement in crystal quality of the films should mainly be due to the high temperature annealing, but since the ratio is larger for the Ce and/or Yb doped films, it can be hypothesized that the RE ions can contribute to the improvement. It has been reported that Ce doping can contribute to a quality improvement [23, 24, 25]. Here the Ce doped film (S5) has the highest I_{NBE}/I_{VIS} ratio, and the Ce + Yb doped sample films (S1-4) have comparable I_{NBE}/I_{VIS} ratios, as predicted by the hypothesis. The RE could contribute to a better crystal quality, or there could be other unknown factors.

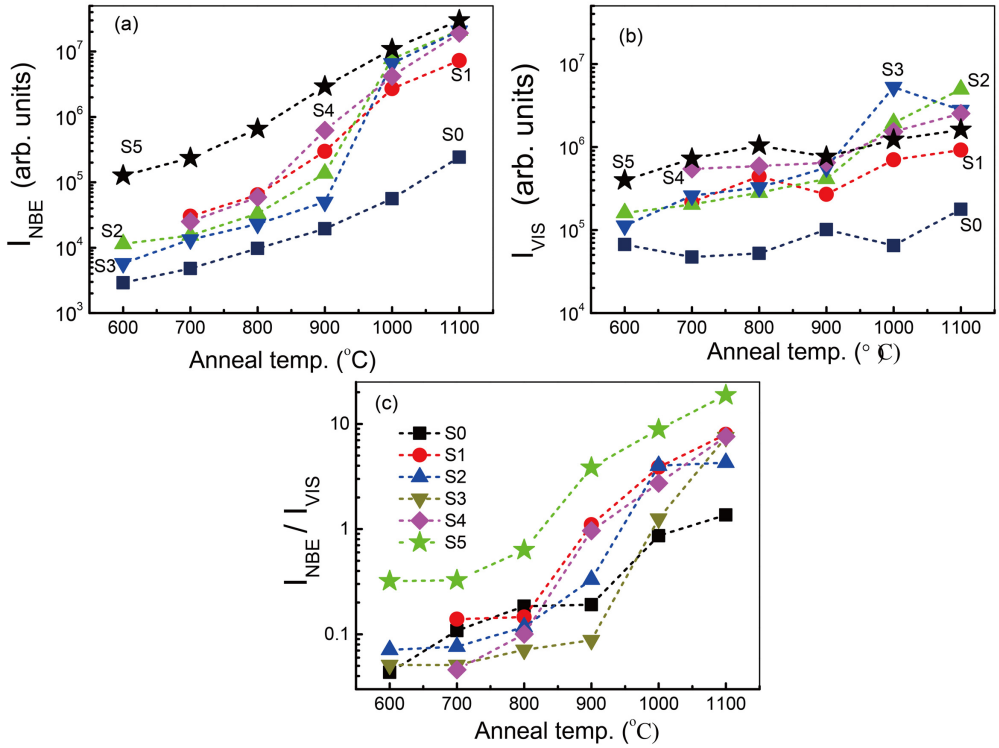

Fig. 2. The integral intensity of (a) the NBE emissions (I_{NBE}, integrated in the range of 350-450 nm) and (b) the visible bands (I_{VIS}, integrated in the range of 450-700 nm) for the S0-5 films as a function of the anneal temperature; (c) the integral intensity ratio of I_{NBE}/I_{VIS} of the films at the indicated temperatures.

The structural evolutions within the S1-5 films caused by the above annealings have been investigated by XRD. The S1, like S0, S4 and S5 has only one dominant peak (2θ ~34.5°) in the XRD spectra corresponding to the diffraction of the (002) plane of ZnO with hexagonal wurtzite structure, and the full-width at half maximum (FWHM) of the (002) peak decreases with increasing anneal temperature. S2 and S3 have more diffraction peaks besides the (002) peak. Figure 3(a) shows the diffraction patterns of S2 after the anneals. For sample S2 after the 600-900 °C annealing, in addition to the (002) diffraction peak, two more diffraction peaks have emerged at 2θ = 31.80° and 36.25°, respectively, corresponding to the diffraction from (100) and (101) planes of ZnO according to JCPDS card number PDF No. 36-1451. The diffraction peaks become sharper after the 1000 °C annealing, indicating that the ZnO nano-particles have increased in size. After the 1100 °C annealing, more peaks emerge in the diffraction pattern. The peaks at 2θ = 12.6, 21.9, 25.4, 31.7 and 36.2° correspond to the formation of Zn_2SiO_4 according to PDF No.37-1485, 19-1479 and 24-1467. The peaks at 2θ = 27.7, 36.2 and 56.6° correspond to the formation of Yb_2SiO_5 and $Yb_2Si_2O_7$ silicates according to PDF No. 37-0458 and 30-1440. The presence of Ce-related oxides or silicates in the films

Optical Materials EXPRESS

cannot be excluded, but the amount is below the detection limit in the present cases. Figure 3(b) compares the XRD patterns of S0-5 after an identical 1100 °C annealing to examine the effects of Ce and/or Yb doping. The inset in Fig. 3(b) plots the FWHM of the (002) peak for the S0, S1, S4 and S5. The width has decreased from 0.181° to 0.172°, then to 0.162° and 0.159°. This infers that the Ce-doped ZnO film has the best film quality among the samples, which is consistent with the above PL measurements. Sample S2 has higher concentration of Ce and Yb than S1. It seems reasonable that the diffraction analysis indicated that zinc and ytterbium silicates have formed in sample S2 and not in S1. Sample S3 has the highest Ce and Yb concentrations of the films. As a natural consequence, the diffraction peaks in the silicate patterns become sharper which means more Yb and Zn silicates have precipitated.

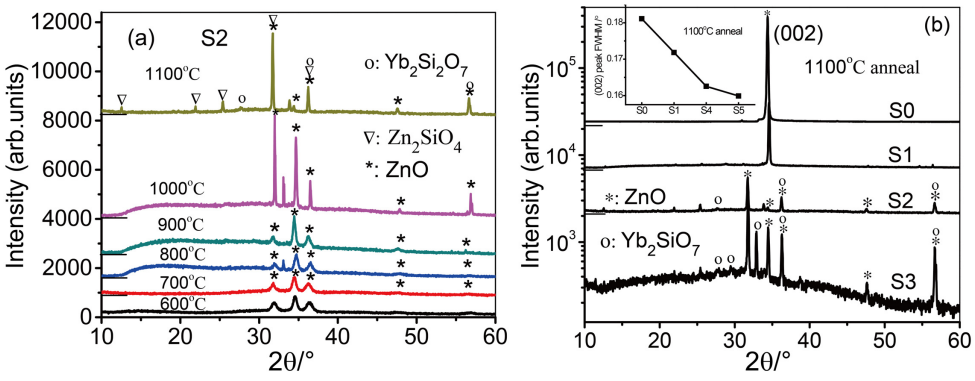

Fig. 3. The XRD patterns of (a) S2 film after annealing at the indicated temperatures; (b) S0, S1-3 films after the same 1100 °C annealing. The inset in (b) is the FWHM of (002) diffraction peaks for the S0, S1, S4 and S5 films.

The surface morphology of the films before and after high temperatures annealing were studied by SEM. Figure 4 shows the SEM images of S0-S3 as-deposited (A.D.) or annealed at 1100 °C for 30 minutes. The surface morphologies of S5 were reported in Ref. 19, the SEM images of S5 are similar to those reported in Ref. 20, and thus both are not shown here.

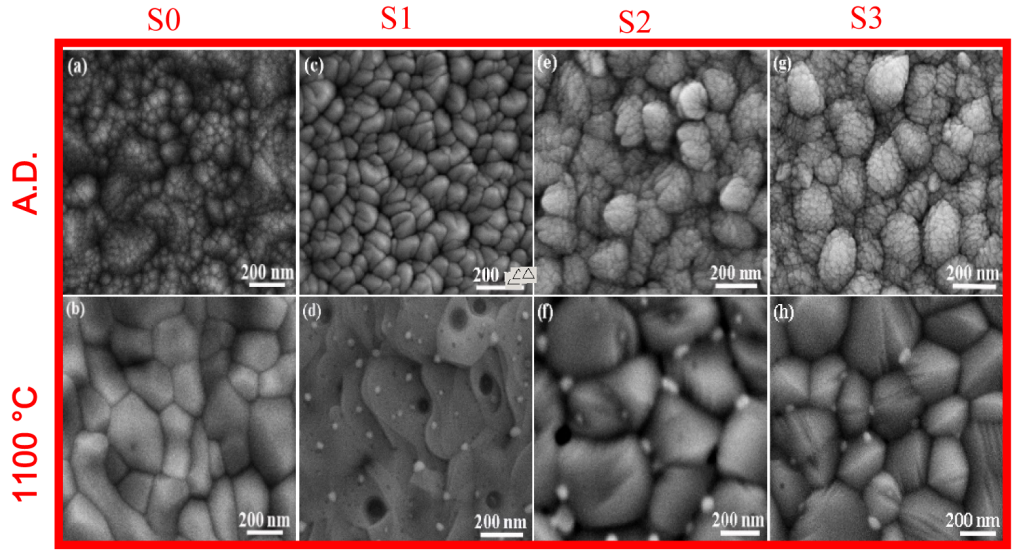

Fig. 4. Surface morphologies of the samples: (a), (c), (e) and (g) are as-deposited S0, S1, S2, and S3 films, respectively; (b), (d), (f), and (h) are 1100°C annealing S0, S1, S2, and S3 films, respectively.

Optical Materials EXPRESS

In Fig. 4(a), the A.D. S0 is composed of tiny ball-shaped particles with sizes in dozens of nm, but most of the particles have aggregated. After annealing (Fig. 4(b)), the particles coalesced to form big nanocrystals with different shapes. The particles in A.D. S1 are more uniformly distributed but have irregular shapes as shown in Fig. 4(c). After annealing the particles have also coalesced into a denser film matrix, but there are many precipitates seen as white dots on the film surface (Fig. 4(d)). EDS analysis indicates that the dots have higher oxygen and Yb content but lower Zn content in comparison with the matrix locations (not shown), which means the dots could be Yb_2O_3 nanoparticles. Precipitations were also reported by Jiang et al [26] and Ye et al [27] in Yb-doped ZnO films and also attributed to the formation of crystal Yb_2O_3 precipitates. In addition to the dots, one can see hole-shaped nanostructures in the annealed film. This phenomenon could result from diffusion processes that reduce the stress/strain of the films [19]. Figure 4(e) shows the surface image of A.D. S2. Compared to Fig. 4(c), the particles look like pinecones which are composed of many tiny ZnO crystallites. After annealing (Fig. 4(f)), the "pinecone" structures have developed into smooth nanocrystals (several hundred nanometers) with a clear boundary. Larger Yb_2O_3 nanoparticles have precipitated but mainly at the boundary of the nanocrystals, and the hole-shaped structures become less pronounced. The surface morphologies of S3 (A.D. and 1100 °C anneal) are similar to those of S2 as is shown in Figs. 4(g) and 4(h), respectively.

The strong UV emissions from Ce doped ZnO thin films (S5) after high temperature annealing has been attributed to the improved crystal quality of the films [19]. In [20], we have also reported strong NBE emission from Yb doped ZnO thin films, but the Yb concentration (~5 at.%) is higher than those of S1-S4. Here, the REs doping concentrations are higher than that of the Ce single doping case, and Zn and Yb silicates as well as Yb_2O_3 have formed in the films. Luo et al [18] reported that strong UV lasing occurred in their Eu doped ZnO films, where Eu_2O_3 precipitated on the surface of the ZnO host. They proposed that the surface of ZnO is passivated by the outer Eu_2O_3 layer, which acts as energy potential barrier to prevent the surface defects of ZnO nanocrystals from capturing photo-generated electron, and also greatly reduces the concentration of singly ionized oxygen vacancies. A similar situation may be applicable to our case where Yb_2O_3 have precipitated on the films surface. The Zn- and RE-silicates could also play a part in the enhancement of PL intensity by changing the excitation energy concentrations, which could also change the contribution from stimulated emission in the films. Further research on the mechanism for the strong UV enhancements is in progress.

Figure 5 shows the UV PL intensity of the films as a function of the laser excitation power. Generally this dependence can be expressed as $I \propto P^m$, where I is the luminescence intensity, P the excitation power, and m is the number of photons needed for producing an emission photon. The dependence provides information about the mechanisms involved in the luminescence [28]. We report on preliminary characterizations indicating lasing in the following.

Optical Materials EXPRESS

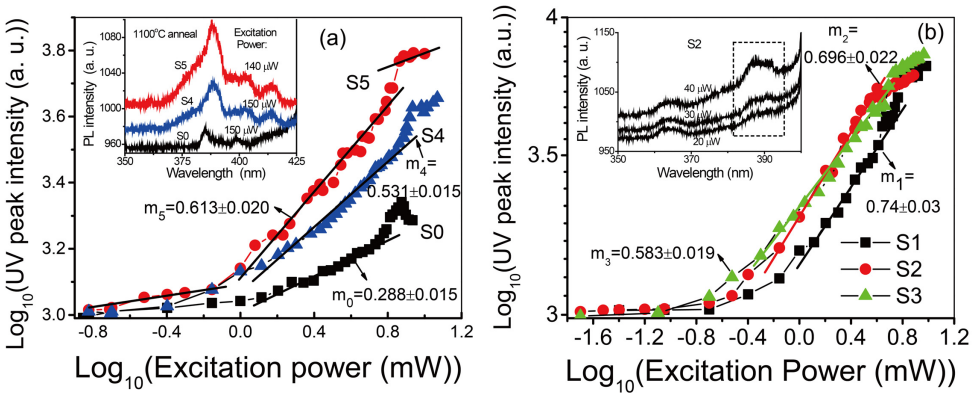

Fig. 5. The peak intensities of the UV PL for (a) S0, S4 and S5 films, and (b) S1, S2 and S3 films as a function of the He-Cd laser excitation power. The sample films were annealed at the identical 1100 °C. The inset in Fig. 5a shows the PL spectrum of S0, S4 and S5 under their excitation powers, while the inset in Fig. 5(b) shows the PL spectra of S2 with increasing the excitation power to 40 μW.

In Fig. 5(a), the UV peak intensities of S0, S4, and S5 all exhibit three specific regimes with different power exponents *m* (see for example S5). The regime with lowest intensity could correspond to the spontaneous emission of ZnO due to exciton recombination, and the regime with drastically increasing intensity may correspond to stimulated emission due to electron-hole plasma recombination, in analogy with the regimes assigned by Luo et al [18]. The intensities tend to saturate for an excitation power around 1.02 W/cm^2, which could be due to some nonlinear optic effects [29]. After a simple power law fitting, the exponents for the stimulated emission regimes of S0, S4 and S5, m are 0.29, 0.53 and 0.61 respectively. The inset in Fig. 5(a) shows the onset of efficient PL spectrum for the S0 film with excitation power of about 150 μW (the onset excitation powers for S4 and S5 are similar to S0). In Fig. 5(b), S1-3 have similar $I \propto P^m$ dependence as those of the control samples. The exponents, *m*, for the stimulated emission regimes of the S1, S2 and S3 are 0.74, 0.70, and 0.58, respectively. The excitation powers of the lasing onset for the of S1-3 have decreased greatly to be about 40 μW, the inset of Fig. 5(b) shows the emerging of the lasing peak of S2 with increasing the pump power to the critical excitation. One see the width of the peak is around 4 nm which is very narrow and indicates that stimulated emission is occurring in the material. The higher RE doping concentration is beneficial to decrease the critical excitation power. We speculate that the decrease of the critical excitation power in S1-3 could be related to the energy coupling between the RE oxide and the ZnO nanoparticles [30]. Further studies on the strong UV enhancement and the excitation mechanism is in progress.

4. Conclusion

In conclusion, we have reported that after 1000-1100 °C annealing, the NBE emissions of (Ce, Yb) co-doped ZnO films were dozens to hundred times stronger than that of undoped ZnO, while the Yb^{3+} emission (~980 nm) was quite weak indicating that energy transfer from the ZnO host to Yb^{3+} ions in the films were not efficient. Structural analysis demonstrated that the high temperature annealing and (Ce,Yb) co-doping, had remarkable effects on the crystallinity and morphology of the films, which are considered to be responsible for the strong NBE enhancements of the co-doped ZnO films. The (Ce, Yb) co-doped ZnO films have relatively lower onset excitation power compared to the undoped ZnO and Ce (or Yb) singly doped ZnO films.

Optical Materials EXPRESS

Funding

Doctoral Fund of Ministry of Education of China (NO. 20111101120021); State Key Laboratory for Artificial Microstructure and Mesoscopic Physics and the State Key Laboratory of Nuclear Physics and Technology, Peking University.